Study of the Internal Structure and Small-Scale Instabilities in the Dense Z Pinch

V. V. Ivanov, J. P. Chittenden, S. D. Altemara, N. Niasse, P. Hakel, R. C. Mancini, D. Papp, and A. A. Anderson

Phys. Rev. Lett. **107**, 165002 — Published 12 October 2011

DOI: 10.1103/PhysRevLett.107.165002

Study of the internal structure and small-scale instabilities in the dense Z pinch

V. V. Ivanov[1], J. P. Chittenden[2], S. D. Altemara[1], N. Niasse[2], P. Hakel[1], R. C. Mancini[1], D. Papp[1], A. A. Anderson[1]
[1]*Department of Physics, University of Nevada, Reno, NV 89557, USA*
[2]*Blackett Laboratory, Imperial College, London SW7 2BZ, UK*
(Dated …

High resolution laser diagnostics at the wavelength of 266 nm were applied for the investigation of Z pinches at the 1-MA generator. The internal structure of the stagnated Z pinches was observed in unprecedented detail. A dense pinch with strong instabilities was seen inside the column of the trailing plasma. Kink instability, disruptions, and micropinches were seen at the peak of the x-ray pulse and later in time. The three-dimensional structure of the stagnated Z pinch depends on the initial wire-array configuration and implosion scenario. Small-scale density perturbations were found in the precursor plasma and in the stagnated Z pinch. Development of instabilities is in agreement with three-dimensional magnetohydro-dynamic simulations.

PACS numbers: 52.58.Lq, 52.59.Qy, 52.35.Py

Dense and hot Z-pinch plasmas are used in a variety of high-energy-density physics application [1-4]. Radiative properties of dense Z-pinches strongly depend on plasma instability which is the primary impediment for the x-ray power yielded by a collapsing z-pinch. Instabilities affect wire-array Z-pinch plasmas at all main phases: ablation, implosion, and stagnation. Inhomogeneity and asymmetries of the imploding plasma [5-7] seed instabilities into the stagnating pinch. Mitigation of plasma inhomogeneity during the implosion phase in multi-wire cylindrical loads and star wire arrays results in enhanced power of x-ray radiation [1,2,8]. The peak power of the Z-pinch is limited by the fast growth of magnetohydrodynamic (MHD) instabilities at the stagnation stage. The stagnated Z-pinch is unstable to both the m=0 sausage and m=1 kink perturbations [3,4]. Another set of features and instabilities in the Z-pinch plasma is linked to "enhanced" plasma heating [9-11]. It has been experimentally established that the radiated energy of Z-pinches can exceed the available kinetic energy and resistive Spitzer heating. Several mechanisms may contribute to Z-pinch energy deposition, including the resistive effect in Hall plasma, the dissipation of the entrained magnetic flux, ion viscous heating, and forced expansion of the m=1 helix [9-13]. Hot spots in Z-pinches with the electron temperature >1 keV and density $>10^{21}$ cm^{-3} [14] can also contribute to the energy balance in the Z-pinch. Some of the expected plasma perturbations are in the scale of 10^{-4}-10^{-3} cm that is less than the typical resolution of optical and x-ray Z-pinch plasma diagnostics. Moreover, laser radiation at 532 nm does not penetrate the trailing material around the pinch due to strong absorption and refraction. The structure of the stagnated Z-pinch has been studied with x-ray self- emission diagnostics, which can derive a temperature map of the pinch with a spatial resolution of 70-150 μm [3]. X-ray radiography was applied to X-pinches, a single wire and ablation and implosion stages in wire-array Z-pinches [6,15,16].

Laser diagnostics for Z-pinch plasma at the ultraviolet (UV) wavelength of 266 nm were developed at the Zebra generator [17]. The critical electron density of plasma at 266 nm is $1.6\cdot10^{22}$ cm^{-3} that is ~100 times higher compare to the pinch electron density at the 1-MA generator. The absorption and refraction in plasma are significantly smaller at the wavelength of 266 nm. A UV laser channel was applied for investigation of the fine structure of the dense Z-pinch.

In this Letter we present the first observation of the small-scale structure of the dense Z-pinch hidden by the trailing material. Strong kink instability, areas of disruption and micropinching, and instability on the pinch edge are observed in stagnated Z-pinches. A position of the micropinch correlates with a bright spot on the x-ray image of the pinch. The stagnation scenario and the three-dimensional (3D) structure of the pinch depend on the wire array configuration. Density perturbations with a scale of 10-30 μm arise in the precursor and stagnated Z-pinch. 3D simulations of instability development carried out with a Gorgon code [13,18] are in agreement with experiments.

The experiments were carried out at the Zebra generator with a 1-MA current pulse, a rising edge of ~80 ns (10 - 90%), and current prepulse of 200 ns [19]. The impedance of the transmission line is 1.9 Ω. A load was installed in the return current cage 8 cm in diameter. The lens objective of the beampath was placed in the vacuum chamber of the generator to increase a spatial resolution. The laser diagnostics included four-frame shadowgraphy at a wavelength of 532 nm [8] and a UV channel at 266 nm. The UV channel included a shadowgraphy and differential interferometry at one time frame with a field of view of 3.5-5 mm. Two lasers generated 0.2 ns laser pulses at wavelengths of 532 and 266 nm each with energy of 50 mJ. The UV laser pulse was synchronized with the first laser pulse of the four-pulse train at 532 nm. Narrowband interference filters blocked self radiation of the Z-pinch plasma on CCD cameras. All laser channels were spatially co-aligned using a removable test object installed in the load during the reference shots. The UV laser diagnostics demonstrates a significant advantage compared to the diagnostics at 532 nm.

Absorption and refraction are much smaller at 266 nm than at 532 nm [17]. The intensity of UV light was increased by the factor of 3-5 during Zebra shots, compared to reference shots, to mitigate absorption in the trailing material surrounding the dense Z-pinch. The trailing mass may contain ~30% of the total load mass in Z-pinches [20]. The spatial resolution of the UV images was limited by the charge-coupled device (CCD) pixel size, 4 μm/pxl. X-ray diagnostics included x-ray diodes and photoconductive detectors, a Ni bolometer, time-gated pinhole camera, and time-integrated spectrometer [11]. The pinhole camera recorded 6x2 frames in two spectral ranges, E > 1 keV and > 3 keV, with a frame duration of 3 ns and spatial resolution of 0.25 mm. Aluminum (alloy 5056) cylindrical and star [8] wire arrays 2 cm tall with masses of 25 - 60 μg/cm were investigated. Cylindrical loads Ø8, 12, and 16 mm and star wire arrays Ø20 mm (two three-ray configurations) and Ø16 mm (a four-ray configuration) were tested.

Figure 1 presents a central part of the cylindrical wire-array Z-pinch at 0.8 ns after the maximum of the x-ray pulse.

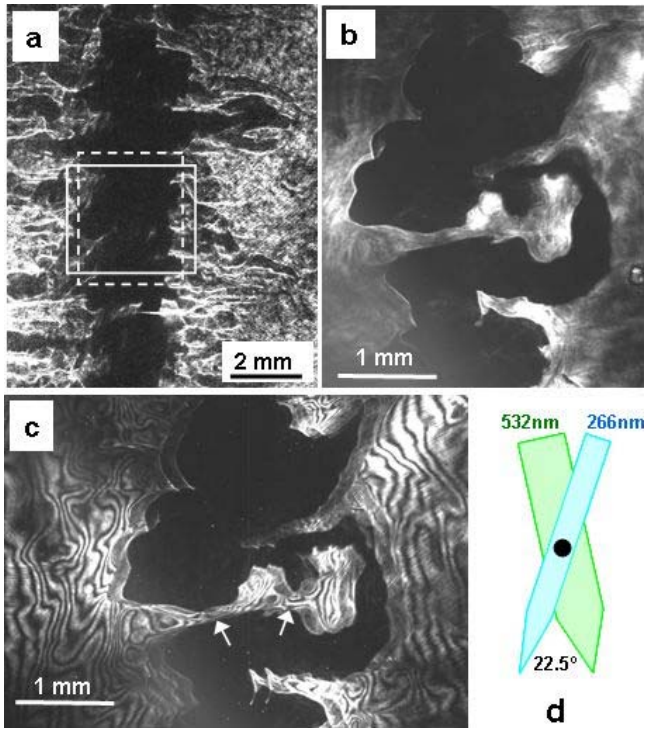

Figure 1. Shadowgrams (a, b) and an interferogram (c) of the central part of the pinch at the wavelengths of 532 nm (a) and 266 nm (b, c). The Z-pinch is produced by the implosion of a cylindrical 16-wire array 8 mm in diameter with a mass of 54 μg/cm, shot 2373. Directions of probing are presented in (d). The cathode is on the top of the images. Shadowgrams (a) and (b) were taken at 0.6 ns after the maximum of the x-ray pulse.

Shadowgram (a) at 532 nm shows an opaque plasma column 2 mm in diameter with flares of non-imploded material and a break in the bottom of the image. Shadowgram (b) at 266 nm presents an area of the dashed rectangle. The angle between these two channels is 22.5º. The UV shadowgram shows strong kink instability with necks 90-150 μm in diameter (or a mix of kink with other perturbations) hidden inside the rectangular area in shadowgram (a). Interferogram (c) at 266 nm presents an area of the solid rectangle in image (a). White arrows in interferogram (c) show squeezed fringes in the gaps. They indicate plasma which may support current in the gaps. This type of the split pinch is a common configuration for wire-array Z-pinches. Strong kink instability exists in all types of tested cylindrical and star loads. The dense Z-pinch has sharp edges in the shadowgram (b) and interferogram (c). Fringes are not seen in the differential shift in (c) due to strong density gradients on the pinch edges.

Strong kink instability and necks increase the current path and resistance and may produce an enhanced heating of the Z pinch. We note that the m=0 perturbations can be stabilized by some methods [4] but Z-pinch is always unstable to m=1 perturbations [21].

Figure 2 presents micropinching in the dense pinch. A neck on the pinch with a diameter of 0.45 mm is seen in

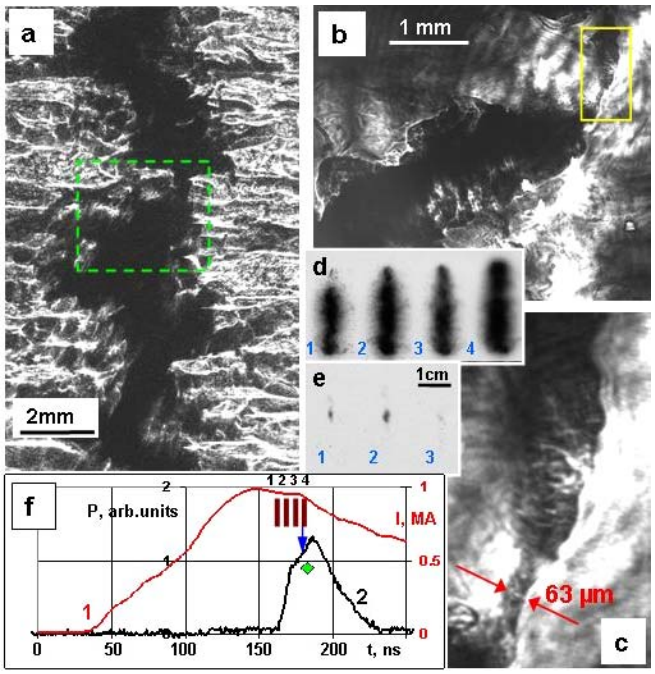

Figure 2 (color online). Shadowgrams at wavelengths of 532 nm (a) and 266 nm (b) are taken in the central area of the Z-pinch. (c) Magnified image of the area marked by the solid rectangle in shadowgram (b). X-ray frames from the pinhole camera filtered for E>0.8 keV (d) and E>3 keV. The diagram (f) presents the timing of the frames at 532 nm (diamond), 266 nm (solid arrow), and x-ray frames (stripes) to the pulse of current (1) and keV x-ray pulse (2). The Z-pinch was produced by implosion of the cylindrical 16-wire array 16 mm in diameter with a mass of 37 μg/cm, shot 2357.

shadowgram (a) at 532 nm. Shadowgrams (a) and (b) were taken at 1.5 ns before the maximum of the x-ray pulse. Shadowgram (b) at 266 nm matches to the dashed rectangle in shadowgram (a) and includes an area of micropinching. The solid rectangle is magnified in image (c) and shows a

micropinch 63 μm in diameter. The micropinch is located inside the plasma neck of the larger diameter, as seen at the wavelength of 532 nm. Small-scale perturbations are seen on the micropinch. X-ray images filtered for energy E>0.8 keV (d) show radiation from the large area. Images (e) with photon energy >3 keV show a bright spot in the center of the pinch. This spot arises on the rising edge of the x-ray pulse and exists for ~10 ns. A position of the bright spot correlates with the micropinch in Fig. 2 (a,b). Micropinches 60-150 μm in diameters were observed in all Al cylindrical arrays and stars Ø20/18.5/17/15.5/14/6 mm. Micropinches with smaller diameters were not found in our experiments. This leads to a suggestion that Al Z-pinches do not collapse to smaller sizes due to the current redistribution [22] or other physical mechanisms.

The 3D structure of the Z pinch at stagnation depends on the configuration of the load. Cylindrical wire arrays implode to a Z-pinch with strong m=0 and m=1 plasma instabilities and bright spots on x-ray images. Kink and sausage instabilities are always seen at the maximum of the x-ray pulse and even on its rising edge. This could be a result of seeding of the implosion bubble-like instability in the wire arrays [7,23] into the pinch. Cylindrical loads Ø16 mm produce an inhomogeneous Z-pinch with a loose structure and necks. The electron temperature T_e of Z pinches was derived from the x-ray spectroscopy of Al K-shell line-emission spectra. The temperature of bright areas on spectra of cylindrical load Ø8 mm was in the range of 400-450 eV while that of low intensity areas was of 320-360 eV. The 3D structure of the pinch may impact the data interpretation because spectra were integrated in time and over a spatial region of 1.5 mm.

A homogeneous dense plasma column ~1 mm in diameter is formed only in the four-ray 24-wire Al star arrays Ø16/14/12/10/8/6 mm. Implosion bubbles are mitigated in star arrays during the cascade implosion [8].

Plasma instability with a period of 70-270 μm was found on the edges of the Z-pinch in several shots. The pinch demonstrates periodical ripple with high plasma gradients on the edges. This perturbation may be associated with the Magneto-Rayleigh-Taylor or flute instability.

A high-resolution UV diagnostic allows investigation of small-scale plasma instabilities in the stagnated Z-pinch. Density perturbations with a scale of 10-30 μm were observed in the precursor plasma during formation of the pinch and in the stagnated dense Z-pinch. Figure 3 displays small-scale density perturbations in shadowgrams at wavelengths of 266 nm. Figure 3 (a) shows the implosion stage in the 16-wire array Ø8 mm at 29 ns before the maximum of the x-ray pulse when plasma is imploding on the array center. A magnified image (b) shows plasma density perturbation in the range of 10-30 μm. Perturbations in the range of 0.3-0.4 mm were observed in the precursor plasma [24] and linked to flute-mode cells initiated by ablating material. Perturbations on smaller scales may be generated in a cascade process. Perturbations in the precursor plasma can induce instability to the main Z pinch.

Figure 3 (c-e) presents small-scale perturbations in the stagnated Z-pinch. UV shadowgram (d) was recorded with enhanced intensity of laser light. The slit was installed before the CCD camera to illuminate a central area of the pinch and block illumination of sides by intensive laser pulse. The intensity of UV light on the slit was increased by a factor of 30 during the Zebra shot for mitigation of light losses in the trailing material and dense pinch. The stagnated dense pinch in image (d) is self-transparent for the UV beam. The intensity of plasma self- emission and refracted stray rays on the pinch image was measured to be < 6% of the intensity of

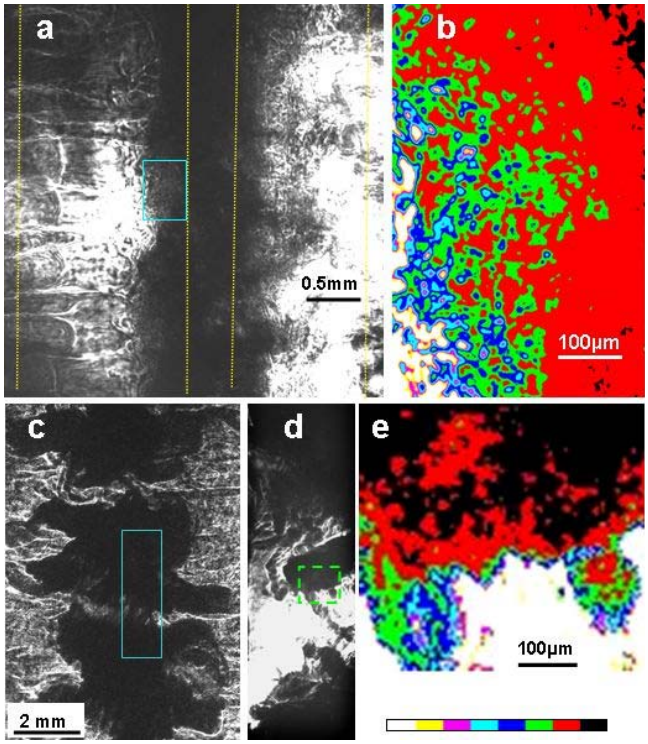

Figure 3 (color online). Small-scale instabilities in the wire-array Z-pinch plasmas. (a) The UV shadowgram at the implosion stage, 29 ns before the maximum of the x-ray pulse in 16-wire cylindrical array Ø8 mm with a mass of 54 μg/cm, shot 2369. Vertical lines show the initial positions of wires in the array. (b) A magnified false-color image from the rectangle in image (a). Shadowgrams (c-e) at 532 nm displays a stagnation stage in the Al 3-ray star array Ø20/18.5/17/15.5/14/6 mm at the maximum of the x-ray pulse, shot 2354. A complementary shadowgram (d) presents a slit area at the same time, with enhanced UV light intensity in 30 times. (e) A magnified false-color image from the dashed rectangle in image (d).

probing radiation. The structure of background laser radiation was recorded on the CCD camera during the reference laser shots. A complementary interferogram recorded a full image taken without slit. Figure 3 (e) shows density perturbations with a size of 10-15 μm in the current-carrying area of the Z-pinch. Small-scale plasma perturbations may be responsible for "enhanced" plasma heating [13]. The origin and role of these plasma instabilities in the Z-pinch energy balance will

be studied in future experiments.

Breaks on the pinch with lower plasma density are seen in Fig. 3 (d), Fig. 1 (a), and other shadowgrams. Breaks can initiate high-energy electron beams and play a role in the energy balance of wire-array Z-pinches. These breaks are observed in cylindrical arrays and stars Ø20 mm.

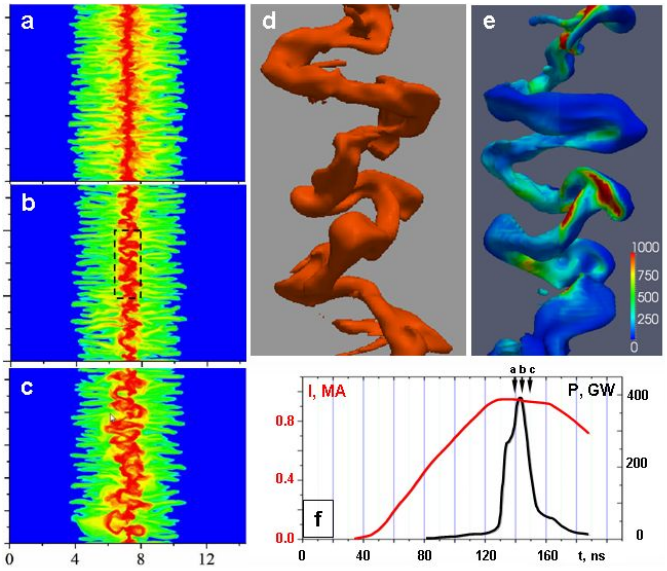

Figure 4 (color online). (a-c) 3D MHD Gorgon simulation of the mass density integrated along the line of sight, in the cylindrical 16-wire array Ø8 mm. (d-e) Magnified 3D surfaces of the high density region (d) and electron temperature of this region (e) from two orthogonal views taken from the dashed rectangle in (d). The timing diagram (f) presents the current pulse (red line), calculated x-ray pulse (black line), and timing of frames (arrows).

Experimental data about the internal structure of the Z pinch make possible benchmarking of 3D MHD codes at the stagnation phase. The stagnation stage in the cylindrical and star wire-arrays was modeled with the 3D resistive MHD code Gorgon [12, 18]. The code was run in with a 15-30 μm spatial grid. The development of instabilities in a cylindrical array Ø8 mm and a 4-ray star wire array were compared with experimental shadowgrams. Figure 4 displays simulations of the electron density distribution, integrated along the line of sight in the Al star wire array Ø8 mm with the mass of 54 μg/cm. Frames (a)-(c) present the evolution of instability in the stagnated Z-pinch. A strong kink perturbation is seen in Fig. 4 (b), (d) and (e) at the maximum of the radiated x-ray pulse. Figure 4 (c) shows rapid growth of kink instability 5 ns later. Figure 4 (d) and (e) show surfaces of constant electron density (10^{21} cm^{-3}) from two orthogonal views. The period and radial amplitude of kink instability are similar to experimental data. The loop-like structures seen in Fig. 1 and other shadowgrams are reproduced in simulations. At this stage, roughly a quarter of the current is flowing through the narrow dense plasma column illustrated in Figures 4 (d) and (e). The electron temperature of the pinch varies from 100 eV in large cold areas up to 1 keV in small hot spots. The local magnetic field associated with this current (200-500 T) drives m=0 instability growth at various points along the column. At the same time, the helical components of the current path generate incoherent regions of axial magnetic field (up to 200 T) which force an expansion of the helix and increase the amplitude of the m=1 instability.

The simulation of the Z-pinch in a four-ray 24-wire star array also agrees well with experiments. Gorgon simulations show a cascading implosion and the formation of a homogeneous dense Z-pinch plasma column without kink instability at the maximum of the x-ray pulse. These dynamics were also observed in experiments. The Gorgon modeling is therefore in good agreement with implosion and stagnation scenarios observed in two very different cylindrical and star wire arrays.

The small-scale structure and perturbations in the stagnated 1-MA Z-pinch were unfolded with high resolution UV laser diagnostics. The 3D structure of the Z pinch is responsible for radiative properties of Z pinches. It should be taken into account for interpretation of the spectroscopic and x-ray imaging data with a limited spatial resolution. The UV laser probing with a temporal framing may also be applied to the stagnated Z pinch at multi-MA generators.

The authors thank Drs. J. M. Kindel and A. M. Covington for support, Dr. D. D. Ryutov for discussions, and A. L. Astanovitskiy, O. Dmitriev, V. Nalajala, and E. McKee for help in experiments. Work was supported by the DOE/NNSA under UNR grant DE-FC52-06NA27616.

1. C. Deeney et al., Phys. Rev. Lett., **81**, 4883 (1998).
2. R. B. Spielman et al., Phys. Plasmas. **5**, 2105 (1998).
3. M. E. Cuneo et al., Phys. Rev. E **71**, 046406 (2005).
4. D. D. Ryutov et al., Rev. Mod. Phys. **72**, 167 (2000).
5. S. V. Lebedev, D. J. Ampleford, S. N. Bland et al., Plasma Phys. Contr. Fusion **47,** A91 (2005).
6. D. B. Sinars et al., Phys. Rev. Lett. **93**, 145002 (2004).
7. V. V. Ivanov et al., Phys. Rev. Lett. **97**, 125001 (2006).
8. V. V. Ivanov et al., Phys. Rev. Lett. **100**, 025004 (2008).
9. C. Deeney et al., Phys. Rev. A **44**, 6762 (1991).
10. A. I. Velikovich et al., Phys. Plasmas **7**, 3265 (2000).
11. V. V. Ivanov et al., Phys. Rev. **E 79**, 056404 (2009).
12. J. P. Chittenden, S. V. Lebedev, C. A. Jennings et al., Plasma Phys. Control. Fusion **46,** B457 (2004).
13. M. G. Haines et al., Phys. Rev. Lett. **96**, 075003 (2006).
14. N. R. Pereira, J. Davis, J. Appl. Phys. **64**, R1 (1988). K. N. Koshelev, N. R. Pereira, J. Appl. Phys. **69**, R21 (1991).
15. D. H. Kalantar, D.A. Hammer, Phys. Rev. Lett. **71**, 3806 (1993).
16. S. A. Pikuz et al., Phys. Rev. Lett., **89**, 035003 (2002),
17. V. V. Ivanov et al., IEEE Trans. Plasma Sci. **38**, 574 (2010).
18. J. P. Chittenden, C. A. Jennings, Phys. Rev. Lett. **101**, 055005 (2008).
19. G. S. Sarkisov et al., Phys. Plasmas **14**, 052704 (2007).
20. S. V. Lebedev et al., Phys. Plasmas **8**, 3734 (2001).
21. J. P. Friedberg, Rev. Mod. Phys. **54**, 801 (1982).
22. G. E. Sarkisov et al., JETP **81**, 743 (1995).
23. B. Jones et al., Phys. Rev. Lett. **95,** 225001 (2005).
24. V.V. Ivanov et al., IEEE Trans. Plasma Sci. **35**, 1170 (2007).